



# DIGITAL ACCESS TO SCHOLARSHIP AT HARVARD

## Wafer-scale metasurface for total power absorption, local field enhancement and single molecule Raman spectroscopy

The Harvard community has made this article openly available.  
[Please share](#) how this access benefits you. Your story matters.

|                          |  |
|--------------------------|--|
| <b>Citation</b>          | Wang, Dongxing, Wenqi Zhu, Michael D. Best, Jon P. Camden, and Kenneth B. Crozier. 2013. "Wafer-scale metasurface for total power absorption, local field enhancement and single molecule Raman spectroscopy." <i>Scientific Reports</i> 3 (1): 2867. doi:10.1038/srep02867. <a href="http://dx.doi.org/10.1038/srep02867">http://dx.doi.org/10.1038/srep02867</a> . |
| <b>Published Version</b> | <a href="https://doi.org/10.1038/srep02867">doi:10.1038/srep02867</a>  |
| <b>Accessed</b>          | February 19, 2015 2:39:51 PM EST   |
| <b>Citable Link</b>      | <a href="http://nrs.harvard.edu/urn-3:HUL.InstRepos:11878868">http://nrs.harvard.edu/urn-3:HUL.InstRepos:11878868</a>  |
| <b>Terms of Use</b>      | This article was downloaded from Harvard University's DASH repository, and is made available under the terms and conditions applicable to Other Posted Material, as set forth at <a href="http://nrs.harvard.edu/urn-3:HUL.InstRepos:dash.current.terms-of-use#LAA">http://nrs.harvard.edu/urn-3:HUL.InstRepos:dash.current.terms-of-use#LAA</a>                     |

*(Article begins on next page)*



OPEN

SUBJECT AREAS:

METAMATERIALS

NANOPARTICLES

RAMAN SPECTROSCOPY

NANOPHOTONICS AND  
PLASMONICS

Received

13 May 2013

Accepted

18 September 2013

Published

4 October 2013

Correspondence and  
requests for materials  
should be addressed to  
K.B.C. (kcrozier@seas.  
harvard.edu)

# Wafer-scale metasurface for total power absorption, local field enhancement and single molecule Raman spectroscopy

Dongxing Wang<sup>1</sup>, Wenqi Zhu<sup>1</sup>, Michael D. Best<sup>2</sup>, Jon P. Camden<sup>2</sup> & Kenneth B. Crozier<sup>1</sup>

<sup>1</sup>School of Engineering and Applied Sciences, Harvard University, Cambridge, MA, 02138, USA, <sup>2</sup>Department of Chemistry, University of Tennessee, Knoxville, TN, 37996-1600, USA.

The ability to detect molecules at low concentrations is highly desired for applications that range from basic science to healthcare. Considerable interest also exists for ultrathin materials with high optical absorption, e.g. for microbolometers and thermal emitters. Metal nanostructures present opportunities to achieve both purposes. Metal nanoparticles can generate gigantic field enhancements, sufficient for the Raman spectroscopy of single molecules. Thin layers containing metal nanostructures (“metasurfaces”) can achieve near-total power absorption at visible and near-infrared wavelengths. Thus far, however, both aims (i.e. single molecule Raman and total power absorption) have only been achieved using metal nanostructures produced by techniques (high resolution lithography or colloidal synthesis) that are complex and/or difficult to implement over large areas. Here, we demonstrate a metasurface that achieves the near-perfect absorption of visible-wavelength light and enables the Raman spectroscopy of single molecules. Our metasurface is fabricated using thin film depositions, and is of unprecedented (wafer-scale) extent.

The realization of strong and tunable optical absorption is advantageous for applications that include photon detection<sup>1</sup>, solar energy conversion<sup>2</sup>, and photo-induced water splitting<sup>3</sup>. Previous studies<sup>4–9</sup> have shown that metasurfaces enable efficient optical absorption at visible and infrared wavelengths. With the exception of Ref. 9, however, their fabrication involved electron beam lithography, a time-consuming and costly method that is only suitable over small areas (usually <1 mm<sup>2</sup>). Ref. 9 aimed to address this by instead employing silver nanocubes, but their chemical synthesis is by no means straightforward. Here, we report the realization of metasurfaces with near-complete absorption and record areas (4 inch wafers, i.e. ~80 cm<sup>2</sup>) using standard sputtering and evaporation techniques. These consist of silver nanoparticle islands formed over a silver mirror, with an SiO<sub>2</sub> spacer layer, and are termed “SIOM metasurfaces”. We show that their reflectance can be tuned by adjusting parameters that include the spacer thickness and the evaporation rate, which in turn modifies the silver nanoparticle island morphology. We discuss the physical interpretation of the perfect absorption phenomenon in terms of equivalent electric and magnetic surface currents. These are enabled by the SIOM metasurface supporting both electric and magnetic resonances. The perfect absorption behavior is accompanied by huge local field enhancement that is advantageous for surface-enhanced Raman scattering (SERS)<sup>10–13</sup>. We perform SERS measurements of molecules adsorbed to the SIOM metasurfaces and determine the enhancement factors (EFs), i.e. the factors by which the Raman signals from molecules on the SIOM metasurface are increased compared to molecules in the pure liquid form (i.e. no metasurface). We find that the SIOM metasurfaces exhibit EFs that are more than one order of magnitude larger than those of silver nanoparticle islands on glass. We furthermore demonstrate, for the first time, single molecule SERS with a metasurface. The large extent of our SIOM metasurface enables the observation of an unprecedented number (>7000) of single molecule SERS events.

## Results

The SIOM metasurface we introduce is schematically illustrated as Figure 1a. The starting substrate is silicon, onto which silver and SiO<sub>2</sub> layers are deposited by evaporation and sputtering, respectively. Silver nanoparticle islands are then formed by evaporating silver at a slow rate. Further details are provided in the Methods section. We note that our approach involves no complex or expensive fabrication procedures, and is inherently suitable for the producing substrates with large areas. Indeed, the SIOM metasurfaces are on 4 inch wafers (Figure 1b), only limited by the sizes of the holders in our evaporator and sputterer. We furthermore note that we choose to employ a Si wafer as the underlying substrate for convenience. The silver mirror, however, is of sufficient

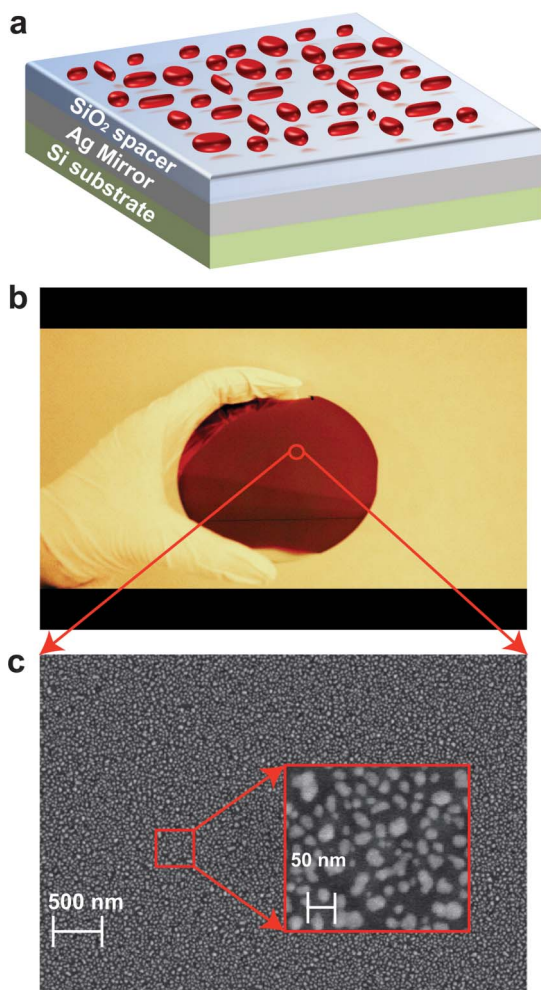


**Figure 1 | SIOM metasurface.** (a). Schematic of SIOM metasurface. Silver nanoparticle islands (depicted as red particles) are deposited on a 50 nm-thick SiO<sub>2</sub> spacer above a 120 nm-thick silver mirror. Silicon is used as supporting substrate. (b). Image of fabricated SIOM metasurface with a diameter of 4 inches. (c). Scanning electron microscope (SEM) image of a portion of SIOM metasurface. Inset: SEM image of metasurface at higher magnification.

thickness so that there is almost no penetration of light into the Si substrate. The optical properties of the substrate are therefore unimportant, meaning that even more economical substrate materials (e.g. plastic or steel) could be used.

An SEM image of a portion of the SIOM metasurface is shown in Figure 1c. The SEM image verifies that the silver nanoparticle islands are formed on the SiO<sub>2</sub> layer. It is seen from Figure 1b that the fabricated SIOM metasurface appears red in color. To understand this phenomenon, we measure its reflectance (Figure 2a, Methods).

The reflection spectrum (Figure 2a) shows a dip at  $\lambda \approx 525$  nm at which the reflectance is very small. As we discuss further below, the dip is related to the excitation of localized surface plasmons on the silver nanoparticle islands, but these are strongly modified by the presence of the silver mirror. As the reflectance is below 10% over a band extending from  $\lambda \approx 450$  nm to 600 nm, the SIOM appears red in color (Figure 2b). To understand the origin of the reflection spectrum dip, we analyze the sizes of the nanoparticle islands. We randomly pick a  $5 \mu\text{m} \times 3.5 \mu\text{m}$  region from the SEM of the SIOM substrate, import the image into MATLAB (The Mathworks Inc.), and find the effective radius of each silver nanoparticle island within this region. The effective radius is the radius of a circle that would have the same area as the area of the nanoparticle island, as found

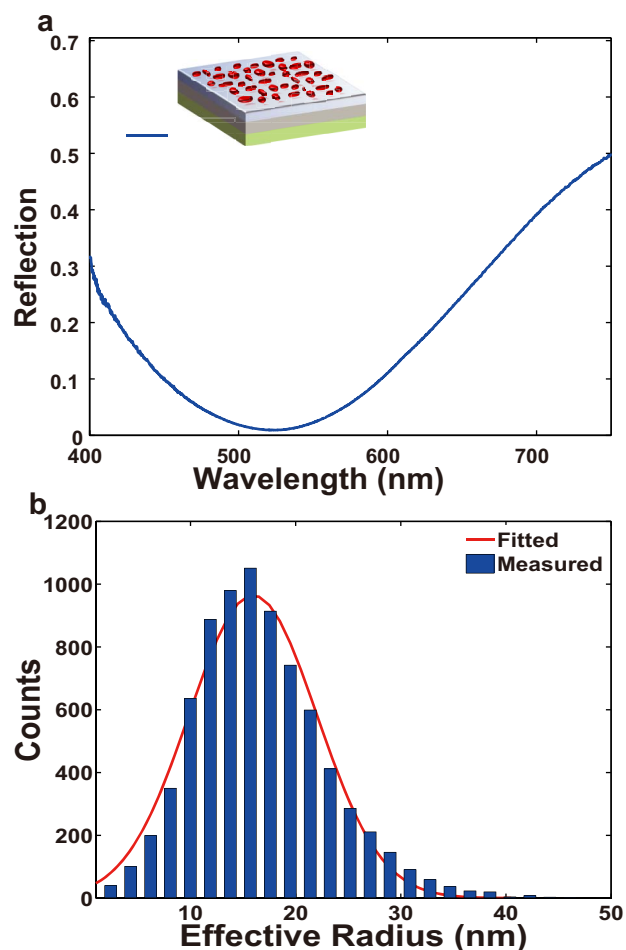


**Figure 2 |** (a). Reflection spectra of SIOM metasurface. (b). Histogram of effective radii of silver nanoparticle islands of SIOM metasurface.

from analysis of the SEM image. The effective radii found in this way are tabulated in a histogram (Figure 2b), and can be seen to follow a Gaussian distribution (red fitted curve) that peaks at an effective radius of 15.4 nm and has a standard deviation of 6 nm. We check other areas of the SIOM substrate and obtain similar results. It is likely that this size dispersion contributes to the broad width of the reflection dip.

From Figure 2a, it can be seen that reflectance from the SIOM substrate is very low, being below 1% at a wavelength of  $\lambda = 525$  nm. Indeed, the SIOM metasurface achieves near total power absorption. The perfect absorption phenomenon can be interpreted as arising from the metasurface inducing equivalent magnetic and electric surface currents that produce far-fields that interfere destructively<sup>9</sup>. To explore this interpretation, we randomly choose a  $1 \mu\text{m} \times 1 \mu\text{m}$  region of the SEM of Figure 1c, and simulate the fields under plane wave illumination using the finite difference time domain (FDTD) method. The equivalent magnetic and electric surface currents are found from the field distribution using the surface equivalence theorem<sup>14</sup>. These current distributions are shown as Figure S1 of the Supplementary Materials. It can be seen that the regions of enhanced electric currents are co-located with those of the enhanced magnetic currents. This originates from the SIOM metasurface simultaneously supporting electric and magnetic resonances; we discuss this point further below. These results show that, at the simulated resonance of  $\lambda = 530$  nm, the total effective magnetic and electric currents, i.e. each integrated over the unit cell, are in a ratio  $(383 + 1.2i)$  ohm, i.e. each integrated over the unit cell, are in a ratio (383 + 1.2i ohm) that is close to 377 ohm, i.e. the impedance of free space. As discussed further in the Supplementary Materials, the results therefore predict



destructive cancellation of the far-fields produced by these currents, leading to the total absorption phenomenon. We furthermore note that the reflection spectrum predicted by the simulation is in very reasonable agreement with the experimentally-measured spectrum (Figure S1b of Supplementary Materials).

The simultaneous existence of magnetic and electric resonances has been previously studied in relation to total absorption<sup>15</sup>. To further explore the near-total absorption achieved by the SIOM substrate, we study a simplified model consisting of a silver disk (radius 29 nm) formed on a silver mirror, with an SiO<sub>2</sub> spacer layer (50 nm thick) between them. The disks are assumed to be on a square lattice (340 nm period). The results (Figure S2, Supplementary Materials) reveal that a current loop is formed between silver islands and mirror when illuminated at  $\lambda = 525$  nm, meaning that the structure has a magnetic resonance. It can also be seen that an electric resonance occurs at the same wavelength (Figure S2b, Supplementary Materials). These resonances generate equivalent electric and magnetic surface currents that (Figure S3, Supplementary Materials), when integrated over a unit cell, are in a ratio (381 + 7i ohm) very close to 377 ohm, meaning that near-total absorption is also predicted for the simplified SIOM metasurface. This is discussed in further detail in the Supplementary Materials.

The SIOM metasurface reflectance spectrum is readily tuned by modifying the fabrication process. Varying the evaporation rate presents a means for doing this, as it in turn modifies the sizes of the nanoparticle islands that are produced<sup>16,17</sup>. In Figure S4 (Supplementary Material), the reflectance spectra of SIOM metasurfaces produced with different silver evaporation rates are shown. It can be seen that increasing the evaporation rate red-shifts the reflectance dip position, which indicates the silver nanoparticle islands increase in size with evaporation rate. Annealing after deposition is another means for modifying the sizes of the silver nanoparticle islands<sup>18,19</sup>. One would also expect that modifying the thickness of the SiO<sub>2</sub> layer would permit the reflectance spectrum to be tuned, due to the important role of the nanoparticle island-film coupling in this system. In Figure 3 we show reflectance spectra for SIOM substrates fabricated using methods that are identical, apart from the spacer layer thickness being varied from 30 to 65 nm. It can be seen that the reflectance dip blue-shifts with increasing spacer layer thickness. This is in agreement with the previous theoretical studies<sup>20,21</sup> that show that the coupling between an optical antenna and mirror (i.e. silver mirror here) reduces with their separation, leading to a blue-shift of the plasmon resonance.

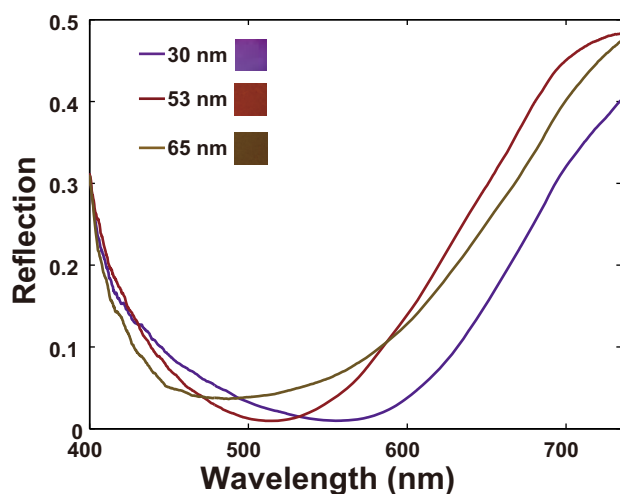


**Figure 3** | Reflection spectra of SIOM metasurfaces having SiO<sub>2</sub> spacer layers with thicknesses of 30 nm, 53 nm and 65 nm. Inset: images of fabricated SIOM with different thicknesses of SiO<sub>2</sub> layer.

Because our SIOM metasurface achieve near-total optical absorption in a very thin region at its surface, it is intuitive to expect that huge local field enhancement will occur around the silver island nanoparticles. This makes it an ideal candidate for SERS. SERS substrates patterned with high resolution lithography (e.g. e-beam) achieve very high performance and reproducibility<sup>22–29</sup>, but have high cost and small active areas. For many applications, however, large area and low cost are critical. This has motivated the development of SERS substrates patterned by methods other than high resolution lithography, e.g. with nanomaterials such as nanospheres<sup>30,31</sup> or nanoshells<sup>32</sup>. Our SIOM metasurfaces, however, present further advantages in this regard, however, as their fabrication does not involve lithography, nor the use of nanomaterials, but rather standard thin film deposition methods. The SIOM metasurface generates larger SERS enhancements than its simpler counterpart that consists of silver islands on an SiO<sub>2</sub> substrate. This can be understood by considering the excitation and scattered fields in the SERS process. The SIOM metasurface achieves near-total absorption, meaning that the coupling between excitation fields and the plasmonic resonance of the silver islands is more efficient for the SIOM metasurface than for the simpler SERS substrates (silver islands on glass). For the SIOM metasurface, therefore, the field enhancement of the excitation is stronger. This is confirmed by simulations of the electric field intensities produced by the SIOM and by its counterpart consisting of silver islands on glass (Figure S5, Supplementary Materials). The simulation results reveal that SIOM generates peak electric field intensities about  $\sim 3.3$  times larger than those produced by silver islands on glass. In addition to enhancement of the incident field, the silver mirror reshapes the SERS emission patterns so that the emission is mostly radiated into air<sup>26,33</sup>, rather than into the substrate.

For comparison purposes, we characterize the SERS performance not only of our SIOM metasurfaces (Figure 1b), but also that of a substrate consisting of silver nanoparticle islands on indium tin oxide coated glass. The latter is fabricated by evaporating silver at the same rate as that used for the SIOM metasurface. This produces silver nanoparticle islands very similar to those of the SIOM metasurface, as confirmed by scanning electron microscopy (Figure S6, Supplementary Materials). Both types of samples are coated with benzenethiol, and SERS measurements are performed (further details in Methods section) under identical conditions. The results (Figure 4a) show that the SERS signals (and hence signal-to-noise ratios) of all Raman lines are much larger for the SIOM metasurface than for the silver island nanoparticles on glass. This indicates that the SIOM metasurface produces considerably stronger SERS enhancements than do the silver nanoparticle islands on SiO<sub>2</sub>. To quantify the improvement, we analyze the 1072 cm<sup>-1</sup> and 1586 cm<sup>-1</sup> Raman lines. The SERS enhancement factor of these two Raman lines for the SIOM metasurface and the silver nanoparticle islands on glass are calculated by comparing the SERS measurements of Figure 4a with measurements made on pure benzenethiol liquid using the technique shown in a previous study<sup>24</sup> and described in the Methods section.

The experimentally-determined SERS enhancement factors of the 1072 cm<sup>-1</sup> and 1586 cm<sup>-1</sup> Raman lines of the SIOM metasurface are  $4.3 \times 10^7$ , and  $4.4 \times 10^7$ , respectively. By contrast, for the same Raman lines, the silver island nanoparticles on glass exhibit measured enhancement factors of  $2.5 \times 10^6$  and  $1.8 \times 10^6$ . The enhancement factors of the 1072 cm<sup>-1</sup> and 1586 cm<sup>-1</sup> Raman lines of the SIOM metasurface are therefore respectively 17 and 24 times larger than those of the silver island nanoparticles on glass. The more than one order of magnitude boost in enhancement factor results from improvement in the coupling between the incident light and plasmon resonance of the SIOM metasurface. The Raman scattering is furthermore efficiently collected due to the presence of the silver mirror.

We next investigate the uniformity in SERS enhancement with position on the SIOM metasurface. A 300  $\mu\text{m} \times 300 \mu\text{m}$  region of



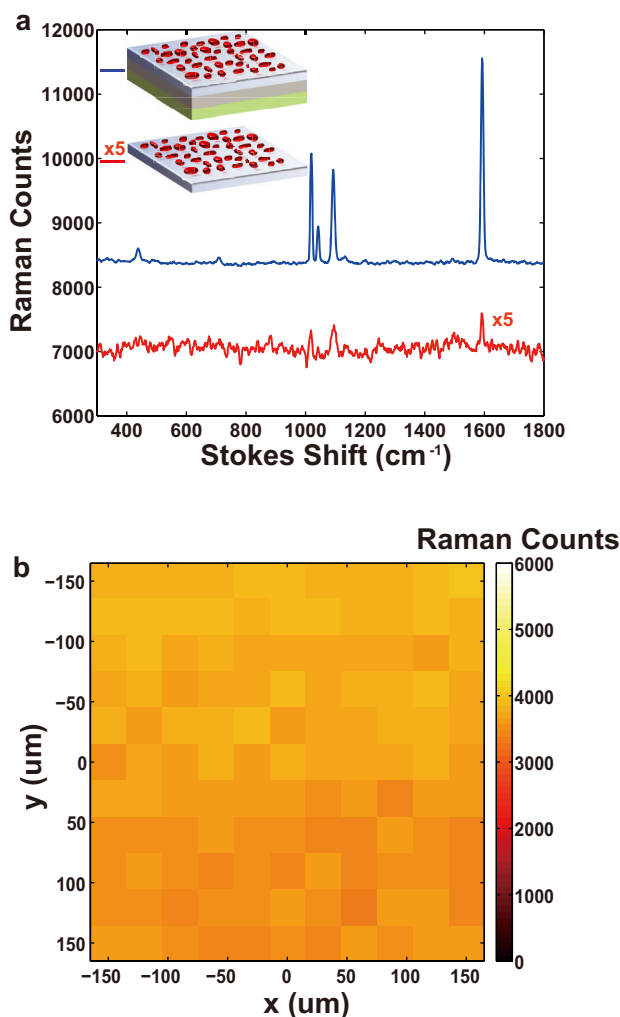


**Figure 4 | SERS measurement.** (a). SERS spectra measured from SIOM metasurface (blue line) and silver island nanoparticles on SiO<sub>2</sub> (red line) coated with benzenethiol. For display purposes, Raman spectrum from SIOM metasurface is shifted vertically by 7000 Raman counts and Raman spectrum from silver nanoparticle islands on glass is enlarged by 5 times. (b). Mapping of SERS signal of 1586 cm<sup>-1</sup> Raman line over SIOM metasurface. Plotted quantity is intensity of 1586 cm<sup>-1</sup> Raman line with background subtracted.

the SIOM metasurface is scanned with a step size of 30 μm, with a SERS spectrum obtained at each stage position. The measurement parameters are described in the Methods section. We plot the intensity of the 1586 cm<sup>-1</sup> Raman line with the background removed as a function of stage position (Figure 4b). It can be seen that the SERS enhancement is very uniform, with the standard deviation being only ~4% of the mean. The other Raman lines and the other regions of the SIOM metasurface also show similar results. We anticipate that the very high degree of uniformity of the SIOM metasurface would be advantageous for many applications.

The initial reports of single molecule SERS (SMSERS)<sup>12,13</sup> garnered considerable interest, but the demonstration of a large area substrate with SMSERS sensitivity has proven elusive. Furthermore, previous reports of SMSERS have been performed almost entirely using aggregates of Ag colloidal nanoparticles that are very heterogeneous, with generally fewer than 1% being SMSERS-active<sup>34</sup>. Here, we demonstrate that our SIOM metasurfaces have SMSERS sensitivity. This is performed using the isotopologue method<sup>35,36</sup>. We introduce two forms of Rhodamine 6G (R6G-d0 and R6G-d4) to the SIOM substrates at low concentration (0.2 nM). As discussed further

below, this allows us to prove that the SERS spectra we then measure are predominantly from single molecules.

The isotopologue method we use for verifying that SMSERS is achieved<sup>35</sup> employs two forms of Rhodamine 6G that differ only in the isotopic composition of their atoms, with the hydrogen atoms in R6G-d0 being replaced by deuterium atoms in R6G-d4. The isotopologues adsorb to the metasurface with identical affinities, yet can be distinguished by shifts in their vibrational features. The Raman line of R6G-d0 at ~620 cm<sup>-1</sup> shifts to ~610 cm<sup>-1</sup> in R6G-d4, for example. This presents a means for determining whether a measured SERS spectrum originates from one or from both types of molecules. If the SMSERS regime has been achieved, and the SERS spectra are from predominantly single molecules, then these spectra should indicate the presence of chiefly one isotopologue (R6G-d0 or R6G-d4), with both types of molecules being simultaneously present only infrequently.

After the R6G isotopologues are introduced, the SIOM metasurface is scanned and SERS measurements are made (see Methods section). Measurements are made at 50625 stage positions, of which 7059 yield spectra that clearly contain Raman features. The criterion for a spectrum containing Raman features is that the height of the Raman peak (after background subtraction) is larger than the sum of the average value and one standard deviation. The average value and standard deviation are found from analysis of the spectra obtained at all 50625 stage positions. Representative spectra are included as Figure 5a. Each measured SERS spectrum is classified into one of three categories: it contains no R6G features, or it contains only R6G-d0 features, or it contains only R6G-d4 features, or it contains both R6G-d0 and d4 features. The results are shown as a histogram in Figure 5b. That the measured spectra contain features of both isotopologues simultaneously on an infrequent basis indicates that the SMSERS regime is achieved. This can be further quantified with a Poisson-binomial model<sup>35</sup>. The histogram of Figure 5b shows that the number of events with no molecules (null events), R6G-d0 only, both R6G-d0 and d4, and R6G-d4 events are in a ratio of 43566:3407:267:3385, i.e. a normalized ratio of ~163:12.8:1:12.7. From the SEM of the SIOM metasurface (Figure 1c), it can be seen that many nanoparticles would be within the laser spot employed in the SERS measurements. It is entirely possible, therefore, that within the laser spot, there are general several locations of the SIOM metasurfaces at which the enhancement is sufficiently strong so that SMSERS is possible. One may think of the union of these regions as the hot spot region. A Poisson-Binomial model with on average 0.15 molecules within the hot spot region predicts that 86.1% will contain no molecules, 6.7% will contain only R6G-d0 molecules, 6.7% will contain only R6G-d4 molecules, and 0.52% will contain both R6G-d0 and R6G-d4. Such a model would therefore predict that, for the 50625 measurement points, the numbers with no molecules, R6G-d0 only, both R6G-d0 and d4, and R6G-d4 only would be 43573:3394:264:3394, i.e. a normalized ratio of ~165:12.85:1:12.85. This is in very reasonable agreement with the experimentally-measured ratio, confirming the validity of the model. The model further predicts that the 6.7% of events containing only one isotopologue comprises 6.45% having solely one molecule, with the remaining 0.25% having two or more molecules. One may therefore conclude that ~96.3% of SERS spectra containing features of only one isotopologue originate from a single molecule, with the remaining ~3.7% originating from two or more molecules.

## Discussion

In conclusion, we demonstrate a visible-wavelength metasurface that achieves near-total power absorption and exhibits single molecule sensitivity. Our SIOM metasurface consists of silver nanoparticle islands over a silver mirror, and is therefore readily fabricated on a wafer-scale using standard thin film depositions. The SIOM metasurface supports magnetic and electric resonances. These can be considered to generate effective electric and magnetic currents that

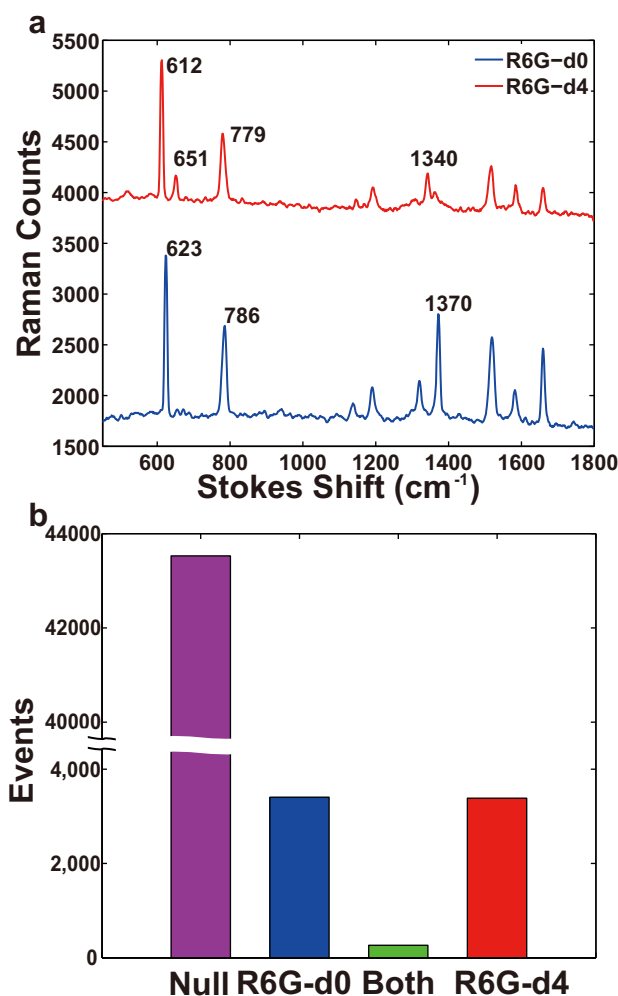


**Figure 5 | Experimental results of SMSERS on SIOM metasurface.** (a). Representative Raman spectra of R6G-d0 molecule and R6G-d4 molecule at single molecule level. R6G-d4 spectrum is shifted vertically by 2000 counts for display purposes. (b). Histogram of single molecule level events: null (purple), R6G-d0 molecule only (blue), both R6G-d0 and R6G-d4 molecules (green), and R6G-d4 molecule only (red).

generate far-fields that cancel, leading to zero reflection and complete absorption. We show that the spectral properties of the SIOM metasurface can be tuned by modifying its geometry via changing the fabrication parameters. As one might intuitively expect, the total absorption property is accompanied by very strong local field enhancement. We demonstrate that this is highly advantageous for SERS. Measurements show that our SIOM metasurfaces exhibit SERS enhancement factors that are more than one order of magnitude higher than those of silver nanoparticle islands on glass. The results also demonstrate a very high degree of uniformity over the SIOM substrate, with the standard deviation in SERS signal being only  $\sim 4\%$  of the mean. We demonstrate that the high enhancement factor permits the detection of the Raman spectra of single molecules. Due to the uniformity of our SIOM substrate and its large area, we are able to present an unparalleled number ( $>7000$ ) of single molecule events. We anticipate that, due to their high performance, large area, and low fabrication cost, SIOM metasurfaces could be highly appropriate for many applications in SERS, such as food safety monitoring<sup>37–39</sup>, explosive detection<sup>40,41</sup>, and pharmaceutical quality control<sup>142,43</sup>.

## Methods

**Fabrication.** The fabrication of SIOM metasurface begins with evaporation (1 Å/sec) of titanium to a thickness of 5 nm on a silicon substrate to form an adhesion layer.

After this, silver is deposited to a thickness of 120 nm on the titanium layer by evaporation (1 Å/sec). A 50-nm thick SiO<sub>2</sub> layer is then deposited by sputtering (0.4 Å/sec). Silver is then evaporated at a slow rate (0.2 Å/sec), thereby producing silver nanoparticle islands. The duration of this evaporation step is such that the amount of silver deposited is equivalent to the amount that would be contained in 6.5 nm thick film, as measured by crystal oscillation monitor. These four steps complete the fabrication of the SIOM metasurface.

**Reflection spectra measurement.** In the reflection spectra measurements, the SIOM metasurface is illuminated by light from a halogen lamp focused by a microscope objective (NA = 0.15, magnification 5 $\times$ ). The reflected light from the metasurface is collected by the same objective lens and analyzed by the spectrometer equipped with a thermoelectrically-cooled charge couple device (CCD). The reflected light from an area of the same sample containing only the SiO<sub>2</sub> spacer and silver mirror (i.e. no silver nanoparticle islands) is measured as reference. The normalized reflection spectrum is then found by dividing the spectrum measured from the SIOM by the reference spectrum. This is then multiplied by the theoretical reflection spectrum of the sample containing only the SiO<sub>2</sub> spacer and silver mirror found using the method of Ref. 14. This yields the SIOM reflection spectrum in absolute terms.

**SERS measurement.** The SERS measurement with benzenethiol are performed as follows. The samples are immersed in a solution of benzenethiol in ethanol ( $3 \times 10^{-3}$  mol/L) for 1 hour. This results in a self-assembled monolayer of benzenethiol on the silver islands. After removal from the benzenethiol solution, the samples are rinsed in ethanol and blown dry with nitrogen. SERS measurements are made with a Raman microscope (Horiba Jobin Yvon, LabRam) equipped with a spectrometer and a thermoelectrically-cooled charge coupled device (CCD). The excitation laser wavelength is  $\lambda = 532$  nm and the power impinging upon the substrate is 0.03 mW. These parameters are used for the measurements both on the SIOM metasurface and on the silver nanoparticle islands on glass. An objective lens (NA = 0.15, magnification 5 $\times$ ) is used to focus the excitation laser on the sample and collect the emitted Raman signals. The signal accumulation time for the CCD detector is 10 seconds.

For the SMSERS measurement, the SIOM substrate is soaked in a solution containing the isotopologues R6G-d0 and R6G-d4 in methanol (0.2 nM each) for 12 hours, washed in methanol, then blown dry with nitrogen. The SIOM substrate is then scanned in the Raman microscope with a step size of 4  $\mu\text{m}$  across an 896  $\mu\text{m} \times 896 \mu\text{m}$  region of SIOM metasurface. In the microscope, a laser beam ( $\lambda = 532$  nm) is focused onto the substrate with a microscope objective (NA = 0.9, magnification 100 $\times$ ). The laser power incident on the chip is 0.03 mW. The same objective lens is used to collect the Raman signal into a spectrometer equipped with CCD sensor. The integration time of acquiring the Raman spectrum for each scan position is 0.5 seconds.

**SERS enhancement factor.** Measurements are made of Raman scattering from pure benzenethiol liquid sandwiched between a microscope slide and a coverslip. The benzenethiol thickness (500  $\mu\text{m}$ ) is defined using a spacer to separate the slide and coverslip. The SERS enhancement factor is then given by  $EF = \frac{I_{SERS}/N_{SERS}}{I_{REF}/N_{REF}}$ , where  $I_{SERS}$  and  $I_{REF}$  are the signal intensities measured in the SERS and Raman experiments, respectively. These intensities are the heights of the Raman lines in the spectra with the background subtracted.  $N_{SERS}$  and  $N_{REF}$  are the numbers of molecules in the SERS and Raman experiments, respectively.  $N_{SERS}$  is given by the area of the exposed silver surfaces of the SIOM substrate or simple silver islands multiplied by the packing density of benzenethiol ( $6.8 \times 10^{14} \text{ cm}^{-2}$ )<sup>44</sup>. To estimate the area of the exposed silver surfaces, we model each silver nanoparticle island as a cylindrical pillar whose radius is chosen to yield a cross sectional area matching that of the silver nanoparticle island, as determined from the SEM image. According to the measurements made using a crystal oscillation monitor, the amount of silver deposited is equivalent to that contained in a 6.5 nm thick film. The heights of the pillars are therefore estimated by equating their volume to that of a 6.5 nm thick film. For the SIOM metasurface shown in Figure 1c for example, this yields an estimated height of 14 nm. The estimated surface area of the exposed silver surfaces is taken as the areas of the tops and sides of the cylinders.  $N_{REF}$  is given by the confocal collection volume of the microscope multiplied by the density of pure benzenethiol (9.8 mol/L). The collection volume is found by measuring the Raman signal from a silicon wafer as a function of its position along the optical axis<sup>24</sup>.

- Niesler, F. B. P., Gansel, J. K., Fischbach, S. & Wegener, M. Metamaterial metal-based bolometers. *Appl. Phys. Lett.* **100**, 203508 (2012).
- Zhu, J. *et al.* Optical absorption enhancement in amorphous silicon nanowire and nanocone arrays. *Nano Lett.* **9**, 279–82 (2009).
- Thomann, I. *et al.* Plasmon enhanced solar-to-fuel energy conversion. *Nano Lett.* **11**, 3440–6 (2011).
- Hao, J. *et al.* High performance optical absorber based on a plasmonic metamaterial. *Appl. Phys. Lett.* **96**, 251104 (2010).
- Avitzour, Y., Urzhumov, Y. & Shvets, G. Wide-angle infrared absorber based on a negative-index plasmonic metamaterial. *Phys. Rev. B* **79**, 045131 (2009).
- Liu, N., Mesch, M., Weiss, T., Hentschel, M. & Giessen, H. Infrared perfect absorber and its application as plasmonic sensor. *Nano Lett.* **10**, 2342–8 (2010).



7. Wu, C. *et al.* Large-area wide-angle spectrally selective plasmonic absorber. *Phys. Rev. B* **84**, 1–7 (2011).
8. Tittl, A. *et al.* Palladium-based plasmonic perfect absorber in the visible wavelength range and its application to hydrogen sensing. *Nano Lett.* **11**, 4366–9 (2011).
9. Moreau, A. *et al.* Controlled-reflectance surfaces with film-coupled colloidal nanoantennas. *Nature* **492**, 86–89 (2012).
10. Fleischmann, M., Hendra, P. J., McQuillan, A. J. Raman spectra of pyridine absorbed at a silver electrode. *Chem. Phys. Lett.* **26**, 163–6 (1974).
11. Jeanmaire, D. L. & Van Duyne, R. P. Surface Raman electrochemistry part I. heterocyclic, aromatic and aliphatic amines adsorbed on the anodized silver electrode. *J. Electroanal. Chem. and Interfacial Electrochem.* **84**, 1–20 (1977).
12. Nie, S. & Emory, S. R. Probing single molecules and single nanoparticles by surface-enhanced Raman scattering. *Science* **275**, 1102–1106 (1997).
13. Kneipp, K. *et al.* Single molecule detection using surface-enhanced Raman scattering (SERS). *Phys. Rev. Lett.* **78**, 1667–1670 (1997).
14. Kong, J. A. *Electromagnetic wave theory.* (Wiley, 1990).
15. Dayal, G. & Ramakrishna, S. Design of highly absorbing metamaterials for Infrared frequencies. *Opt. Express* **20**, 17503–17508 (2012).
16. Nishikawa, Y., Nagasawa, T., Fujiwara, K. & Osawa, M. Silver island films for surface-enhanced infrared absorption spectroscopy: effect of island morphology on the absorption enhancement. *Vib. Spectrosc.* **6**, 43–53 (1993).
17. Aroca, R., Ross, D. & Domingo, C. Surface-Enhanced Infrared Spectroscopy. *Appl. Spectrosc.* **58**, 324A–338A (2004).
18. Wang, Q. *et al.* Plasmonic-enhanced quantum efficiency of europium complex using annealed silver island films. *J. Opt. Soc. Am. B* **28**, 220–4 (2011).
19. Royer, P., Goudonnet, J. P., Warmack, R. J. & Ferrell, T. L. Substrate effects on surface-plasmon spectra in metal-island film. *Phys. Rev. B* **35**, 3753–3759 (1987).
20. Lévêque, G. & Martin, O. J. F. Tunable composite nanoparticle for plasmonics. *Opt. Lett.* **31**, 2750–2 (2006).
21. Lévêque, G. & Martin, O. J. F. Optical interactions in a plasmonic particle coupled to a metallic film. *Opt. Express* **14**, 9971–81 (2006).
22. Crozier, K. B., Sundaramurthy, A., Kino, G. S. & Quate, C. F. Optical antennas: Resonators for local field enhancement. *J. Appl. Phys.* **94**, 4632–4642 (2003).
23. Banaee, M. G. & Crozier, K. B. Gold nanorings as substrates for surface-enhanced Raman scattering. *Opt. Lett.* **35**, 760–2 (2010).
24. Chu, Y., Banaee, M. G. & Crozier, K. B. Double-Resonance plasmon substrates for surface-enhanced Raman scattering stokes frequencies. *ACS Nano* **4**, 2804–2810 (2010).
25. Zhu, W., Banaee, M. G., Wang, D., Chu, Y. & Crozier, K. B. Lithographically fabricated optical antennas with gaps well below 10 nm. *Small* **7**, 1761–6 (2011).
26. Wang, D., Zhu, W., Chu, Y. & Crozier, K. B. High directivity optical antenna substrates for surface enhanced Raman scattering. *Adv. Mater.* **24**, 4376–80 (2012).
27. Seok, T. J. *et al.* Radiation engineering of optical antennas for maximum field enhancement. *Nano Lett.* **11**, 2606–10 (2011).
28. Smythe, E., Dickey, M., Bao, J., Whitesides, G. M. & Capasso, F. Optical antenna arrays on a fiber facet for in situ surface-enhanced Raman scattering detection. *Nano Lett.* **9**, 1132–1138 (2009).
29. Zhang, W., Fischer, H., Schmid, T., Zenobi, R. & Martin, O. J. F. Mode-Selective Surface-Enhanced Raman Spectroscopy Using Nanofabricated Plasmonic Dipole Antennas. *J. Phys. Chem. C* **113**, 14672–14675 (2009).
30. Biggs, K. B., Camden, J. P., Anker, J. N. & Van Duyne, R. P. Surface-enhanced Raman spectroscopy of benzenethiol adsorbed on the gas phase onto silver film over nanosphere surfaces: determination of the sticking probability and detection limit time. *J. Phys. Chem. A* **113**, 4581–6 (2009).
31. Ormonde, A. D., Hicks, E. C. M., Castillo, J. & Van Duyne, R. P. Nanosphere lithography: fabrication of large-area Ag nanoparticle arrays by convective self-assembly and their characterization by scanning UV-visible extinction spectroscopy. *Langmuir* **20**, 6927–31 (2004).
32. Jackson, J. B., Westcott, S. L., Hirsch, L. R., West, J. L. & Halas, N. J. Controlling the surface enhanced Raman effect via the nanoshell geometry. *Appl. Phys. Lett.* **82**, 257 (2003).
33. Ahmed, A. & Gordon, R. Directivity enhanced Raman spectroscopy using nanoantennas. *Nano Lett.* **11**, 1800–3 (2011).
34. Camden, J. P. *et al.* Probing the structure of single-molecule surface-enhanced Raman scattering hot spots. *J. Amer. Chem. Soc.* **130**, 12616–7 (2008).
35. Dieringer, J. A., Lettan, R. B., Scheidt, K. A. & Van Duyne, R. P. A frequency domain existence proof of single-molecule surface-enhanced Raman spectroscopy. *J. Amer. Chem. Soc.* **129**, 16249–56 (2007).
36. Kleinman, S. L. *et al.* Single-molecule surface-enhanced Raman spectroscopy of crystal violet isotopologues: theory and experiment. *J. Amer. Chem. Soc.* **133**, 4115–22 (2011).
37. Liu, Y. *et al.* Potential of Raman spectroscopy and imaging methods for rapid and routine screening of the presence of melamine in animal feed and foods. *Appl. Spectrosc.* **63**, 477–480 (2009).
38. He, L. *Application of surface enhanced Raman spectroscopy to food safety issues.* 148 (ProQuest, UMI Dissertation Publishing: 2012).
39. Qin, J., Chao, K. & Kim, M. S. Raman chemical imaging system for food safety and quality inspection. *T. ASABE* **53**, 1873–1882 (2010).
40. Cheng, C., Li, Z., Liu, W. & Wu, J. Stand-Off explosives detection based on Raman spectroscopy. *CORD Conf. Proc.* 1–4 (2010).
41. Izake, E. L. Forensic and homeland security applications of modern portable Raman spectroscopy. *Forensic Sci. Int.* **202**, 1–8 (2010).
42. Vankeirsbilck, T. *et al.* Applications of Raman spectroscopy in pharmaceutical analysis. *TrAC Trends Anal. Chem.* **21**, 869–877 (2002).
43. Wartewig, S. & Neubert, R. H. H. Pharmaceutical applications of Mid-IR and Raman spectroscopy. *Adv. Drug Deliv. Rev.* **57**, 1144–70 (2005).
44. McFarland, A. D., Young, M. A., Dieringer, J. A. & Van Duyne, R. P. Wavelength-scanned surface-enhanced Raman excitation spectroscopy. *J. Phys. Chem. B* **109**, 11279–85 (2005).

## Acknowledgments

This work was supported by the National Science Foundation (NSF, grant numbers ECCS-0747560 and ECCS-1201687), the Harvard Quantum Optics Center, and by the Center for Excitonics, an Energy Frontier Research Center funded by the U.S. Department of Energy, Office of Science and Office of Basic Energy Sciences under Award Number DE-SC0001088. This work was also supported by the UT/ORNL Joint Institute for Advanced Materials, and the U.S. Department of Energy, Office of Basic Energy Sciences, under Award Number DESC0004792 (J.P.C.) and the National Science Foundation under Awards CHE-0954297 and DMR-0906752 (M.D.B.). Fabrication work was carried out in the Harvard Center for Nanoscale Systems, which is supported by the NSF.

## Author contributions

D.W., W.Z., J.P.C. and K.B.C. developed the concept. D.W. performed fabrication and simulations. D.W. and W.Z. performed experiments and data analysis. J.P.C. and M.D.B. produced and characterized the isotopologues. D.W. and K.B.C. wrote the manuscript.

## Additional information

**Supplementary information** accompanies this paper at <http://www.nature.com/scientificreports>

**Competing financial interests:** The authors declare no competing financial interests.

**How to cite this article:** Wang, D., Zhu, W., Best, M.D., Camden, J.P. & Crozier, K.B. Wafer-scale metasurface for total power absorption, local field enhancement and single molecule Raman spectroscopy. *Sci. Rep.* **3**, 2867; DOI:10.1038/srep02867 (2013).



This work is licensed under a Creative Commons Attribution-NonCommercial-NoDerivs 3.0 Unported license. To view a copy of this license, visit <http://creativecommons.org/licenses/by-nc-nd/3.0>